

# Superparamagnetic Iron Oxide Nanoparticle-Labeled Extracellular Vesicles for Magnetic Resonance Imaging of Ischemic Stroke

Shannon Helsper, Xuegang Yuan, Richard Jeske, Jamini Bhagu, Colin Esmonde, Leanne Duke, Li Sun, Yan Li,\* and Samuel C. Grant\*



Cite This: *ACS Appl. Nano Mater.* 2024, 7, 24160–24171



Read Online

ACCESS |



Metrics & More



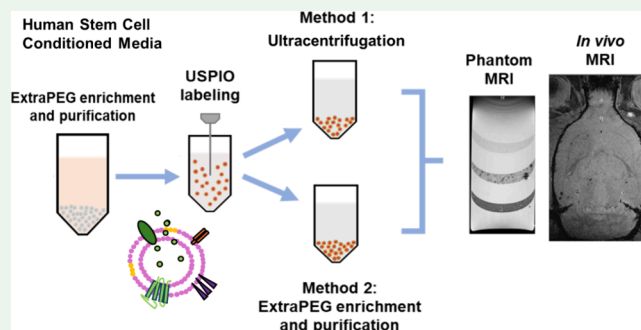
Article Recommendations



Supporting Information

**ABSTRACT:** Stroke is a leading cause of death and disability worldwide. Extracellular vesicles (EVs) derived from human mesenchymal stem cells (hMSCs) offer a unique and promising alternative to direct cell injection as part of a cell-based therapy for stroke treatment. The development of labeling strategies is essential to identifying the initial biodistribution and clearance of EV-based therapeutics. In this study, hMSC-EVs were labeled with ultrasmall superparamagnetic iron oxide (USPIO) nanoparticles for magnetic resonance imaging (MRI). Two methods of preparation were evaluated after EVs were sonicated in the presence of USPIO nanoparticles. The labeled EVs were purified by (1) ultracentrifugation only or (2) an extension of a harvesting approach that employs poly(ethylene glycol) (PEG) to enrich EVs. Following *in vitro* assessment, labeled EVs were applied to an ischemic stroke model and imaged both immediately and longitudinally using MRI. *In vitro* assessment showed the EV characteristics after USPIO nanoparticle labeling. The PEG method exhibited a 3.6-fold enhancement in contrast by using an equivalent USPIO concentration of 0.5 mg/mL and equivalent acquisition parameters (TE = 3.5 ms, TR = 5 s) when the dilution factor is considered. Sufficient USPIO nanoparticle labeling was achieved to visualize the initial biodistribution and assess the initial therapeutic potential. Taken together, simultaneous USPIO nanoparticle labeling and EV enrichment with PEG enhanced MRI contrast and improved outcomes with respect to delivery and ischemic stroke recovery.

**KEYWORDS:** extracellular vesicles, human mesenchymal stem cells, superparamagnetic iron oxide, MRI, preclinical ischemia



## 1. INTRODUCTION

Extracellular vesicles (EVs) are phospholipid vesicles derived from the endosomal membrane of nearly all cell types and play an important role in intercellular communication and the transport of cellular derivatives.<sup>1–3</sup> EV size and composition categorize these bioactive substrates further, namely into exosomes, microvesicles, and apoptotic bodies, although the overlap in diameter and lack of specific markers to each subpopulation make clear separation difficult.<sup>1,4,5</sup> Recently, EVs derived from human mesenchymal stem cells (hMSCs) have been investigated for use in neurodegenerative applications as alternatives to direct cellular implantation due to their paracrine effects,<sup>6</sup> potential for secretome delivery,<sup>7</sup> comparatively low immunogenicity, and ability to cross the blood–brain barrier.<sup>8,9</sup> Preclinical studies have demonstrated EVs as potential therapeutics, particularly in cancer applications<sup>10</sup> and more recently in stroke.<sup>7,11–13</sup> However, knowledge of their initial biodistribution and response to pathology remains limited, in part due to the sparse application of labeled EVs to such disease models. Several imaging modalities have been pursued to overcome this limitation, including computed

tomography imaging,<sup>14,15</sup> bioluminescence,<sup>16</sup> and more recently, magnetic resonance imaging (MRI).<sup>17–21</sup>

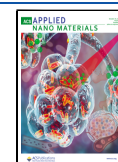
One of the challenges associated with therapeutic imaging is the integration of the labeling or contrast agent while minimizing the disruption of therapeutic integrity, particularly for EVs with fragile coding and noncoding RNA, lipids, and protein cargo.<sup>8,18</sup> Several methods have been under investigation to incorporate labeling agents or other cargo into EVs ranging from incubation to physical treatments.<sup>3,22</sup> While incubation has been successful for small cargo loading, i.e., drugs, it is not suitable for all applications. Although physical treatments, including sonication, rely on membrane disturbance and have the possibility to affect EV cargo, sonication has also been used successfully in EV drug loading<sup>23</sup> and is used in this study to incorporate MRI-compatible contrast agents. MRI

**Received:** August 25, 2024

**Revised:** September 24, 2024

**Accepted:** September 26, 2024

**Published:** October 9, 2024



is already highly accessible in the clinic and routinely used in assessing neurological disease progression such as ischemic stroke. Furthermore, MRI is commonly used to track cell implants with noncytotoxic superparamagnetic iron oxides (SPIO),<sup>24–27</sup> and recent progress has been made to extend this capability to EVs. Although encapsulation of ultrasmall SPIO (USPIO) nanoparticles in EVs for MRI has been reported previously,<sup>17,28,29</sup> particularly for delivery to the kidney, liver, and heart,<sup>18</sup> detection, biodistribution, and clearance of USPIO-labeled EVs in the central nervous system have not been well investigated and yet are critical for novel therapeutic applications in neurology.

Substantial losses of subpopulations incurred during the harvesting step with commercial kits can also compromise the clinical implementation of EVs. As an alternative, recent advancements in EV isolation have employed poly(ethylene glycol) (PEG), an inexpensive yet highly efficient method to increase the yield and integrity of EVs while retaining potentially therapeutic EV populations.<sup>30,31</sup> Although originally designed for EV enrichment, the coupling of this technique following sonication to integrate USPIO allowed simultaneous enrichment and purification of visible MRI EVs compared to ultracentrifugation alone.

In this study, MRI was used to evaluate USPIO nanoparticle-labeled hMSC-EVs using ultracentrifugation only and PEG-based purification methods in phantoms and, subsequently, in a cerebral ischemic stroke rat model. USPIO nanoparticle-labeled EVs in the ischemic hemisphere were confirmed, and initial EV biodistribution and clearance were evaluated using <sup>1</sup>H MRI. Furthermore, recovery of ionic homeostasis within the brain, measured by sodium chemical shift imaging (<sup>23</sup>Na CSI), was used to evaluate the therapeutic potential of the labeled hMSC-EVs. This robust metric is sensitive to the influx of sodium that occurs when the Na<sup>+</sup>/K<sup>+</sup>-ATPase pump is disrupted upon ATP depletion following an ischemic event.<sup>32</sup> Longitudinal <sup>23</sup>Na MRI, as used here, provides key insight into functional recovery in the brain applied to ischemic stroke.<sup>26</sup> This study is the first reported instance of USPIO nanoparticle-labeled hMSC-EV therapy targeting neuropathology and demonstrating functional recovery within an ischemic brain lesion.

## 2. MATERIALS AND METHODS

### 2.1. hMSC Culture and EV-Containing Media Collection.

hMSCs isolated from bone marrow (Tulane Center for Gene Therapy, donor information is shown in Supplemental Table S1) were cultured in complete culture media containing  $\alpha$ -MEM with 10% fetal bovine serum (FBS) (Atlanta Biologicals, Lawrenceville, GA, USA) and 1% penicillin/streptomycin (Life Technologies, Carlsbad, CA, USA) with media change every 3 days. hMSCs were passaged when 80–90% confluency was reached. Cells from passages 4–6 were used for EV collection. The culture medium was replaced with a medium containing EV-depleted FBS for further culture. EV-depleted FBS was generated via ultracentrifugation (100,000g, 18 h) of FBS prior to its use.

To enhance therapeutic significance, hMSCs were cultured under hypoxia for collecting hypoxia-EVs, as previous studies have shown improved stem cell efficacy under low oxygen tension.<sup>33,34</sup> Briefly, cultures in EV-depleted media were placed into a hypoxic chamber under 2% O<sub>2</sub> and 5% CO<sub>2</sub> (BioSpherix Ltd., Parish, NY, USA) for 1 week. Media containing EVs were collected and replaced by fresh media every 2 days. The collected media were preserved at 4 °C for further processing.

**2.2. hMSC-EV Isolation.** EVs were isolated from culture media following a sequential spin (500g for 5 min, 2000g for 10 min, and

10,000g for 30 min) to remove cell debris, apoptotic bodies, large vesicles, etc. Following this, EVs were enriched using the ExtraPEG method as previously outlined<sup>30</sup> by adding 8% (w/v) PEG-6000 to the final supernatant and storing overnight at 4 °C. After spinning the medium/PEG mixture at 3000g for 1 h, the pellet was resuspended in 1 mL of phosphate-buffered saline (PBS) and prepared for ultracentrifugation at 120,000g for 70 min at 4 °C. Following this, the EV pellet was resuspended in 100  $\mu$ L of PBS, and the pellet was disrupted using a benchtop shaker at 1500 rpm for 30 min. The EV sample then was stored at –80 °C until further use.

**2.3. Labeling of EVs with USPIO.** USPIO (average size 5 nm, Fe<sub>3</sub>O<sub>4</sub>, 231.53 g/mol, 5 mg/mL in water; catalog number 725331-5ML, Sigma-Aldrich, St. Louis, MO, USA) was diluted with an hMSC-EV solution to a final volume of 500  $\mu$ L with concentrations of 0.1–0.5 mg/mL. Incorporation of the USPIO was achieved via sonication using a point sonicator (Fisher Scientific, Hampton, NH, USA) in 2 s bursts for 10 s while on ice. This cycle was repeated three times. At this point, samples were randomly assigned to Method 1 or 2.

**Method 1: Ultracentrifugation.** Following sonication, samples underwent a sequential spin series of either (A) 6300g for 30 min to remove free USPIO followed by 39,200g for 30 min to pellet labeled EVs or (B) 9800g for 20 min total to remove free USPIO followed by 27,200g for 20 min to pellet labeled EVs.

**Method 2: PEG enrichment.** Following sonication, another round of the ExtraPEG protocol was used for EV isolation. For washing, the EV pellet was suspended in 1 mL of PBS and underwent 10,000g centrifugation for 30 min at 4 °C. The pellet was suspended in 50  $\mu$ L of PBS for injection or characterization.

**2.4. Nanoparticle Tracking Analysis.** Nanoparticle tracking analysis (NTA) was used to quantify the EV size distribution and concentration. All samples were repeated in triplicate using NanoSight LM10 (NTA 3.4 Build 3.4.003, Salisbury, UK). First, EVs were diluted to 10<sup>8</sup>–10<sup>9</sup> particles per mL with Millipore water. The following parameters were used: camera sCMOS at level 13 and detection threshold set to four. Merged data from the triplicates were calculated for mean, mode, size thresholds D10, D50, and D90 (10, 50, and 90%, respectively), standard deviation, and concentration.

**2.5. Transmission Electron Microscopy (TEM).** EV samples were suspended in filtered PBS for microscopy. Carbon-coated 400 Hex Mesh copper grids (Electron Microscopy Sciences, EMS, Hatfield, PA, USA) were placed on 10  $\mu$ L droplets of EVs or USPIO-labeled EVs for 1 min. Grids were blotted with filter paper to remove the excess sample and washed twice with filtered distilled H<sub>2</sub>O followed by interleaved blot drying. Subsequently, grids were stained with 2% uranyl acetate (EM grade, EMS) for 1 min, dried, and then imaged on a Hitachi HT7800 RuliTEM (Hitachi High Technologies Corp., Tokyo, Japan) at 120 kV. Images were analyzed using ImageJ (NIH, Bethesda, MD, USA) to attain EV size measurements.

**2.6. Protein Quantification and Western Blot.** hMSCs and corresponding EVs were lysed using radio-immunoprecipitation assay buffer (150 mM sodium chloride, 1.0% Triton X-100, 0.5% sodium deoxycholate, 0.1% sodium dodecyl sulfate, 50 mM Tris, and Thermo Scientific Halt Protease Inhibitor Cocktail (Thermo Fisher Scientific, Inc., Waltham, MA, USA)) for 20 min on ice and spun at 14,000g for 20 min. A Bradford assay was carried out to determine the protein concentration on the collected supernatant. Protein lysate concentration was normalized to the lowest concentration, structurally reduced with beta-mercaptoethanol, and boiled at 100 °C in 2 $\times$  Laemmli sample buffer for 5 min. Samples were stored at –20 °C until use. For each sample, 4  $\mu$ g of protein was loaded into wells of 12.5% Bis-Tris-SDS gels and transferred onto a nitrocellulose membrane (Biorad, Hercules, CA, USA). Membranes were blocked for 1 h in 5% skim milk (w/v) in Tris-buffered saline (10 mM Tris-HCl and 150 mM NaCl) with 0.1% Tween 20 (v/v) (TBST). Membranes were incubated overnight in the presence of the primary antibodies in a blocking buffer at 4 °C (1:1000): calnexin (no. 2679) and CD81 (no. 56039, Cell Signaling Technology, Danvers, MA, USA); syntenin-1 (sc-100336) and flotillin-2 (sc-25507, Santa Cruz

Biotechnology, Dallas, TX, USA). Membranes were washed four times with TBST and then incubated with an infrared secondary antibody at 1:5000 for 180 min at room temperature. Blots were washed another four times with TBST and processed by using the LI-COR Odyssey Imaging System (LI-COR, Lincoln, NE, USA).

**2.7. Inductively Coupled Plasma Mass Spectrometry (ICP-MS).** To measure the iron content measurement of USPIO-labeled EVs, ICP-MS was performed. EVs were labeled with 5 mg/mL of USPIO. Concentrations of iron were determined with high-resolution ICP-MS (Finnigan Mat ELEMENT1, Waltham, MA, USA). EV samples were dissolved in 1 mL of 7-N nitric oxide (NO) and dried at 140 °C. The samples then were dissolved in 1 mL of 2% NO and 15  $\mu$ L of indium. Solutions were introduced to the ICP-MS instrument through a 100  $\mu$ L nebulizer and a PFAS Teflon spray chamber (Saville@ Eden Prairie, MN, USA). Plasma power was set at 1200 W. Solutions were measured at intermediate resolution (2500 amu) mode to resolve the  $^{56}\text{Fe}$  peak from  $^{40}\text{Ar}^{16}\text{O}$ . Under these conditions, the intensity peaks have flat tops;  $^{56}\text{Fe}$  was measured at the low-mass side of the peak, as the high-mass side overlaps with the ArO peak. Indium was added to the solution at the 1 ppb level, and indium intensity was used to monitor and correct for plasma drift. For standardization, 2% nitric solutions of 0.5, 1, and 10 ppb iron were used. The concentrations versus intensity of the standard were fitted linearly ( $r^2 = 0.99$ ).

**2.8. miRNA Analysis by Reverse Transcription Polymerase Chain Reaction (RT-PCR).** Total microRNA (miRNA) was isolated from EVs using the miRNeasy Micro Kit (Qiagen, Valencia, CA) according to the manufacturer's protocol. Reverse transcription was carried out using a commercial qScript miR cDNA synthesis kit (Quantabio, Beverly, MA, USA). The qPCR primer was designed and validated to work specifically with PerfeCTa SYBR Green SuperMix using the miRNA cDNA produced. The levels of miR-21, 22, 44, 124, 127, 181, 325, and 1246 were determined. U6 was examined as a housekeeping gene for the normalization of miRNA expression levels. Real-time PCR reactions were performed on a Quantstudio 7 Flex PCR System (Applied Biosystems, Foster City, CA, USA), using a SYBR1 Green PCR Master Mix (Applied Biosystems). The amplification reactions were performed as follows: 10 min at 95 °C and 40 cycles of 95 °C for 15 s and 60 °C for 30 s and 70 °C for 30 s. Fold variation in gene expression was quantified by means of the comparative Ct method:  $2^{-(\Delta C_t \text{ treatment} - \Delta C_t \text{ control})}$ , which is based on the comparison of expression of the target gene (normalized to the endogenous control) between the compared samples.

**2.9. MRI Sample Preparation.** To prepare samples for in vitro MRI, EVs were suspended in a tissue-mimicking phantom composed of agarose gel as previously described.<sup>35</sup> The phantom was made by mixing an equal-volume EV suspension in PBS with 2% (w/w) low-temperature agarose (VWR, Suwanee, GA, USA) to produce a homogeneous gel phase with 1% agarose concentration. Initially, the concentration of labeled EVs ( $\sim 6 \times 10^{10}$ ) for these in vitro studies matched the intended dose to be delivered during in vivo experiments. However, as in vitro MRI contrast was found to be so strong as to prohibit accurate measurement of relaxation, the in vitro concentration of labeled EVs was diluted by a factor of 8 or 16 for Methods 1 and 2, respectively. Regardless, the EV/gel layers within each method preparation contain the same number of labeled EVs. These EV layers were interlaced with pure 1% agarose gel layers in a 10 mm NMR tube. For Method 1, EV layers consisted of initial exposure to 0.5 mg/mL of USPIO with varying centrifugation parameters, as outlined previously. EVs embedded in layers for Method 2 were initially exposed to 0.1, 0.2, or 0.5 mg/mL. As a means of assessing MRI contrast, relaxation decay and saturation recovery experiments were performed at 21.1 T to calculate  $T_2$ ,  $T_2^*$ , and  $T_1$  values.

**2.10. Rat Model of Ischemic Stroke.** All animal procedures were completed in accordance with the NIH Guide for Care and Use of Laboratory Animals and the Animal Care and Use Committee at Florida State University. A transient middle cerebral artery occlusion (MCAO)<sup>36</sup> simulating striatal ischemia was induced in Sprague-Dawley rats (180–225 g) by surgically introducing a rubber-coated

filament in the circle of Willis for 1 h. In brief, rats were anesthetized with 4–5% isoflurane in 100% O<sub>2</sub> and maintained at  $\sim 3\%$  anesthesia for the duration of surgery. A rubber-coated filament (Doccol Corp., Sharon, MA, USA) was inserted into the external carotid artery and threaded 1.9 cm into the internal carotid artery to block the Willis circle, effectively occluding the middle cerebral artery. The filament was secured, and the midline incision was temporarily sutured while the rats regained consciousness in a warmed incubator for the duration of the 1 h occlusion. Following this, rats were reanesthetized, and the filament was removed over the course of 1 min. A microsyringe with a 33-g, 12°-bevel needle (Hamilton, Reno, NV, USA) was used to inject 50  $\mu$ L of labeled EVs ( $\sim 6 \times 10^{10}$  EV) in PBS purified by PEG enrichment ( $n = 3$ ) or ultracentrifugation ( $n = 3$ ) into the internal carotid artery. All rats received pre- and postoperative warming, analgesics (bupivacaine and buprenorphine, respectively), and 10 mL of saline for rehydration over the span of the surgery and day 0 imaging. All animals underwent MR scanning 1–4 h postinjection for initial EV biodistribution evaluation with additional imaging on days 1, 3, and 7. Additional postoperative analgesics and saline were administered following MR on day 1.

**2.11. MRI of Labeled EVs In Vitro and In Vivo.** All MRI experiments were performed at the 21.1 T, 900 MHz vertical MRI scanner at the National High Magnetic Field in Tallahassee, FL, USA.<sup>37</sup> The magnet was equipped with a Bruker Avance III console, and scans were recorded using ParaVision 5.1 (Bruker, Inc., Billerica, MA, USA). A peak gradient strength of 60 G/cm over a 64 cm diameter was provided by the imaging gradient system (Resonance Research Inc., Billerica, MA, USA). For in vitro samples, 10 mm NMR tubes containing the agarose-EV phantoms were loaded into a 10 mm birdcage  $^1\text{H}$  coil tuned to 900 MHz. All scans were acquired at  $(50 \mu\text{m})^2$  in-plane resolution and 0.5 mm slice thickness. High-resolution gradient recalled echo (GRE) images were acquired using TE = 4.0 ms and TR = 1 s with 16 averages for a total scan time of 53 min.  $T_2$  relaxation was assessed using a multislice, multiecho (MSME) spin-echo pulse sequence with an effective TR = 5 s and eight TE times (ranging from 14 to 112 ms in 14 ms increments) with 4 averages for a total scan time of 1.1 h.  $T_2^*$  relaxation was measured using a multiecho GRE sequence with TR = 5 s and ten TE times (3.5 to 62 ms in 6.5 ms increments) with 4 averages resulting in a 50 min total scan time.  $T_1$  relaxation was measured using an MSME with a variable repetition time (TR = 450, 908, 1450, 2111, 2960, 4150, 6150, and 15,000 ms) and an effective TE = 14 ms with two averages for a total scan time of 3.7 h. The acquisition temperature was maintained at 28 °C.

For in vivo experiments, rats were imaged 1 to 4 h following injection of EVs to evaluate the initial EV biodistribution under varying labeling schemes and compared to the injection of EV-free USPIO at the same volume. Additional imaging sessions on days 1, 3, and 7 were completed to assess the clearance of the EV and to evaluate the therapeutic potential. Rats were loaded into a home-built linear birdcage double-tuned  $^{23}\text{Na}/^1\text{H}$  radio frequency coil tuned to 237 and 900 MHz. All rats were oriented in a supine position within the cradle and maintained at or below 3% isoflurane during imaging to ensure a steady respiration rate while in the magnet. Respiration was monitored (Small Animal Instruments, Inc., Stony Brook, NY, USA) and used for acquisition triggering during MRI. EV biodistribution and clearance were confirmed with a  $^1\text{H}$  2D GRE sequence acquired at an in-plane resolution of  $(50 \mu\text{m})^2$  using TE = 4.0 ms and TR = 1 s with one average for a total scan time of 8.5 min.  $T_2$ -weighted images were generated by utilizing a  $^1\text{H}$  2D fast spin echo (FSE) sequence with an in-plane resolution of  $(100 \mu\text{m})^2$  and an effective TE = 2.5 ms and TR = 6 s with one average for a total scan time of 6.5 min.  $^{23}\text{Na}$  MRI utilized a CSI sequence acquired at 1 mm isotropic resolution with TR = 60 ms and 32 min acquisition time.

**2.12. MRI Data Analysis.**  $T_2$ ,  $T_2^*$ , and  $T_1$  values were calculated from their respective relaxation decays and saturation recovery measurements. In brief, regions of interest (ROIs) were defined in ParaVision 5.1 for each EV layer and 1% agarose control. The average signal intensities for each ROI were normalized to the noise baseline and subsequently fitted by nonlinear regression in Prism GraphPad

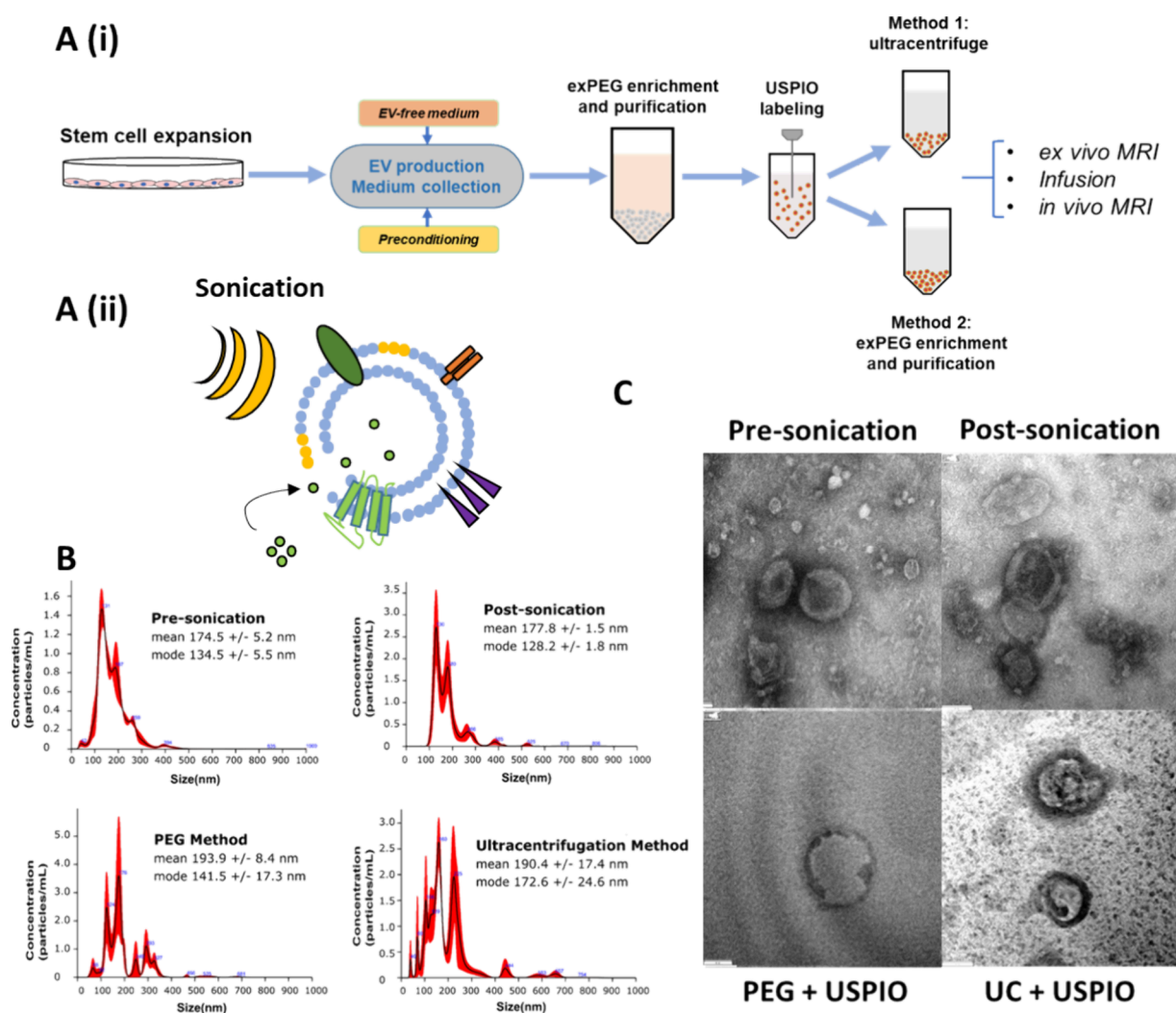


**Figure 1.** Schematic illustration of the labeling process and characterization of EVs after USPIO labeling. (A) (i) Experimental schematic illustration of the labeling process. hMSCs first were expanded under standard culture conditions and then preconditioned under hypoxia. EVs were harvested from hMSC-conditioned media and underwent enrichment and purification by ExtraPEG. Following sonication with USPIO, ultracentrifugation only or an additional ExtraPEG method was used to purify the labeled EVs. (ii) Illustration of the EV sonication process. (B) Size distribution of EVs. EV control (presonation) and postsonication with no label were compared to USPIO-labeled EVs using either ExtraPEG or ultracentrifugation to separate the free USPIO. Representative images of (C) presonation with no label (control), postsonication with no label, and USPIO labeling via the PEG method or ultracentrifugation. Scale bars are equal to 70 nm.

9.2.0 (GraphPad Software, San Diego, CA, USA). For  $T_2$  and  $T_2^*$  values, an exponential decay function was fitted to the data, and values were calculated from their respective  $R_2$  and  $R_2^*$  values according to

$$T_2 = \frac{1}{R_2} \text{ or } T_2^* = \frac{1}{R_2^*} \quad (1)$$

$T_1$  values were extracted in a similar manner using an exponential growth function fitted to the saturation recovery data to determine  $R_1$ .

CSI data reconstructed in MATLAB (MathWorks, Natick, MA, USA) were zero-filled to 0.5 mm isotropic resolution for volumetric and signal analysis in Amira 3D Visualization Software (Thermo Fisher Scientific) as previously described.<sup>27</sup> A signal threshold generated from the contralateral hemisphere was used to define the ischemic lesion:

$$\text{Signal}_{\text{Threshold}} = \text{Signal}_{\text{Contralateral}} + 2.5\text{SSD}_{\text{Contralateral}} \quad (2)$$

All signal above this threshold, excluding CSF, was assigned to the ischemic lesion.

**2.13. Statistical Analysis.** All statistics were performed in Prism GraphPad 9.2.0 using a mixed-effects model with Tukey's multiple

comparison posthoc test. Statistical significance was defined by  $p < 0.05$ .

### 3. RESULTS

#### 3.1. Sonication and Labeling with USPIO Minimally Altered hMSC-EV Characteristics.

EVs were labeled with an MRI contrast agent via sonication to disrupt the EV membrane temporarily, allowing USPIO nanoparticles to be integrated. To minimize the long-term effects of membrane disruption or loss of therapeutic-specific cargo, an optimized procedure was developed combining sonication with ExtraPEG enrichment. This novel method was compared to a more conventional ultracentrifugation-only approach. The experimental schematic is illustrated in Figure 1A. To evaluate the influence of sonication and USPIO labeling or purification steps on the EV properties, the labeled EV size distribution under varying conditions was analyzed using NTA. As demonstrated in Figure 1B, sonication alone slightly altered the EV size distribution profile, decreasing the mode size by ~6 nm. Then,

**Table 1. Iron Content Measurements for USPIO-Labeled EVs**

EV	concentration	number of EV in 100 $\mu\text{L}$	lpg FEI/EV	average lpg FE/EVI
unlabeled #1	$1.70 \times 10^{11}$	$8.33 \times 10^{07}$	$6.75 \times 10^{-09}$	$5.65 \times 10^{-10}$
unlabeled #2	$6.40 \times 10^{11}$	$3.14 \times 10^{08}$	$-1.93 \times 10^{-09}$	
unlabeled #3	$3.50 \times 10^{11}$	$1.72 \times 10^{08}$	$-3.13 \times 10^{-09}$	
labeled 1	$7.80 \times 10^{10}$	$3.82 \times 10^{07}$	$1.14 \times 10^{-06}$	$1.03 \times 10^{-06}$
labeled 2	$5.38 \times 10^{10}$	$2.64 \times 10^{07}$	$8.29 \times 10^{-07}$	
labeled 3	$8.84 \times 10^{10}$	$4.33 \times 10^{07}$	$1.12 \times 10^{-06}$	

USPIO were introduced during the sonication step, and samples were subsequently purified by Method 1: ultracentrifugation only or Method 2: ExtraPEG enrichment. As summarized in Supplemental Table S2, both labeling methods increased the standard deviation of the mean and mode size distributions (8–25 nm vs 2–6 nm). However, processing via the adapted ExtraPEG approach generated EVs with a mode size that was not statistically different from the pre- and postsonication samples, while the ultracentrifugation method resulted in the EVs with a mode size statistically different from the pre- and postsonication samples.

EV size and morphology were then examined using TEM. As seen in Figure 1C, both pre- and postsonication samples with no labeling depicted the typical concave shape of exosomes. Samples incorporating USPIO by ExtraPEG enrichment also demonstrated exosome morphology with the addition of expected contrast due to the MRI-visible nanoparticles, albeit displayed in an extra-vesicular manner. Size measurements conducted on the contrast nanoparticles demonstrated a high correlation to the expected 4–6 nm size of USPIO. EV size distributions determined by TEM are included in Supplemental Figure S1. Using the same approach, the dark spheres within the ultracentrifugation samples also corresponded to the USPIO size. However, significant USPIO nanoparticles were evident outside the EVs in addition to aggregated contrast incorporated into the ultracentrifuged EVs. To confirm that the EVs were labeled with USPIO, ICP was performed to examine the iron content of the labeled EVs (by the PEG method) in comparison to the unlabeled EVs (Table 1). Before labeling, the iron content of the EVs was  $5.65 \times 10^{-10}$  pg Fe per EV. After labeling, the iron content of the EVs was  $1.03 \times 10^{-6}$  pg Fe per EV, showing a 1825-fold increase in iron content.

Total protein was quantified for the EVs pre- and postsonication using a Bradford assay (Supplemental Figure S2). Interestingly, when total protein was normalized to the EV number measured with NTA, a substantial reduction ( $\sim 50\%$ ) in protein for EVs having undergone sonication ( $1.13 \mu\text{g}/10^{10}$  EV) compared to the control group ( $2.24 \mu\text{g}/10^{10}$  EVs) was evident. However, there was no difference between sonication and the PEG method ( $1.12 \mu\text{g}/10^{10}$  EVs) after USPIO were introduced. Furthermore, the ultracentrifugation method exhibited only a minor reduction ( $\sim 12\%$ ) in total protein ( $1.98 \mu\text{g}/10^{10}$  EVs). Specific exosomal protein markers were examined by Western blot for pre- and postsonication samples as well as after labeling via the PEG or ultracentrifugation (UC) method (Figure 2a). Calnexin, an endoplasmic reticulum protein, was used as a negative control to support the absence of cellular debris. Exosome-specific markers CD81 (a membrane-bound tetraspanin protein),<sup>4,28</sup> syntenin-1 (exosome biogenesis protein),<sup>38</sup> and flotillin-2 (a general EV population protein) were verified.<sup>38</sup> As demonstrated, only the cell lysate expressed calnexin, suggesting that the EV samples

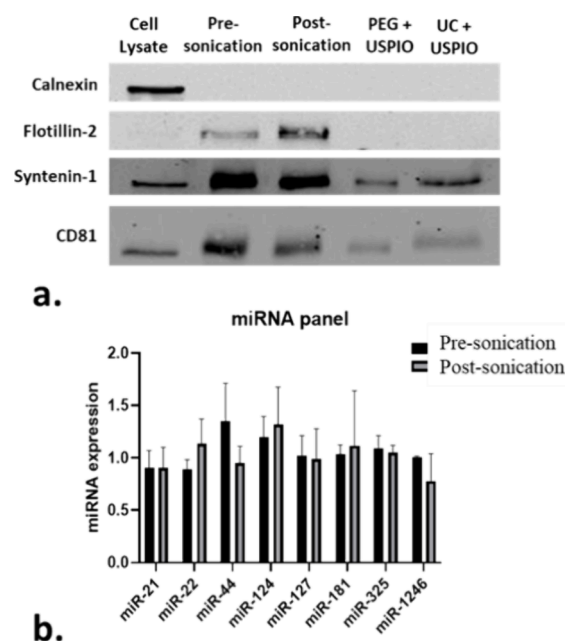


**Figure 2.** Protein and miRNA assessments following the labeling process. (a) Western blot demonstrating expression of exosomal markers under varying processing conditions and (b) miRNA expression pre- and postsonication of hMSC-EVs determined by RT-PCR ( $n = 3$ ).

were free of cellular debris. Although flotillin-2 expression was only verified in the control and sonication samples, CD81 and syntenin-1 were expressed in the control, sonication, PEG and UC samples. The lower expression in USPIO samples may be due to the protein impurity, which was also observed in the cell lysate sample.

As an important functional role, miRNA content in EV cargo was assessed before and after sonication.<sup>39</sup> A panel of miRNA cargo, including miR-21, 22, 44, 124, 127, 181, 325, and 1246 which range from those associated with cell proliferation, apoptosis, and neurogenesis to those having specific roles in ischemia, were analyzed. The expression of these specific miRNAs in the EVs before and after sonication was comparable as determined by RT-PCR (Figures 2b and S3). Notably, elevated levels of brain-specific miR-124 have been found to be a potential indicator for assessment in ischemic patients in addition to miR-21–5p.<sup>40,41</sup> Additional ischemia-related miRNAs could provide insight into the extent of injury or the potential for recovery.

**3.2.  $T_2$  and  $T_2^*$  Maps Demonstrate High Efficiency of USPIO Uptake in EVs.** Sufficient contrast for MRI visualization was established in vitro following exposure to USPIO (0.1, 0.2, or 0.5 mg/mL concentrations) and subsequent processing utilizing ultracentrifugation only (Method 1) or PEG enrichment (Method 2). As in vivo studies were to focus

on neurological applications, labeled EVs were suspended in a 1% agarose gel designed to mimic brain tissue. Apparent  $T_2$  and  $T_2^*$  values were calculated from their respective relaxation decays, and  $T_1$  values were determined from the saturation recovery measurements.

Method 1 compared two centrifugation forces following labeling with 0.5 mg/mL USPIO. Although samples were comparable in signal intensity (Figure 3), the faster centrifuge

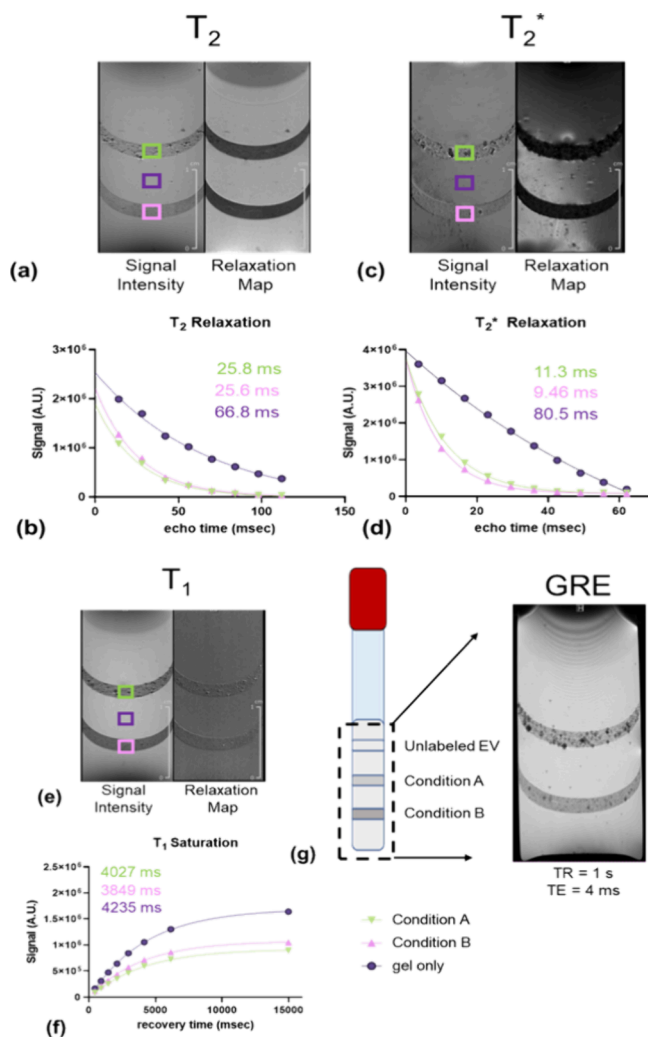


**Figure 3.** MRI of hMSC-EVs labeled and purified via Method 1 suspended in 1% agarose gel. (a,c,e) Signal intensity and relaxation maps for  $T_2$ ,  $T_2^*$ , and  $T_1$ , respectively. (b,d,f) Data fitted to exponential decay or saturation curves. (g) Schematic (left) of EV samples in a 10 mm NMR tube with blank 1% agarose in between layers and GRE image (right) of the NMR tube depicting contrast for the bottom two sample layers only, Condition A and Condition B labeled with 0.5 mg/mL USPIO, and no contrast for unlabeled EVs in the top layer.

speed (Condition A: 39,200g) demonstrated increased aggregation most easily distinguishable in the GRE image (Figure 3). The lower centrifuge force of Condition B (27,200g) displayed a homogeneous layer of labeled EVs. These results align with previous studies that demonstrated increased EV aggregation with higher centrifugation speeds.<sup>5,42</sup> Furthermore,  $T_2$ ,  $T_2^*$ , and  $T_1$  values were comparable between the two ultracentrifugation conditions, exhibiting a  $\sim 61\%$  reduced  $T_2$  value and  $\sim 86\text{--}88\%$  reduced  $T_2^*$  value compared

to gel only. As expected,  $T_1$  values were less affected by the introduction of USPIO to the EVs, exhibiting a reduction of only  $\sim 5\text{--}9\%$ . USPIO primarily affects the transverse relaxation of proximal protons in surrounding areas, therefore generating a strong  $T_2$  or  $T_2^*$  effect. Condition B, corresponding to the lower aggregation of EVs and homogeneity of the in vitro labeling, was deemed to be more suitable for use in subsequent in vivo studies.

Method 2 demonstrated the highest contrast for a 0.5 mg/mL USPIO concentration when compared to 0.1 and 0.2 mg/mL USPIO exposure in 1% agarose gel. Even at a higher dilution factor, the additional PEG enrichment after USPIO incorporation enables enhanced contrast at lower labeling concentrations. An 80% decrease in contrast-to-noise ratio (CNR) compared to the gel was calculated for  $T_2$  (Figure 4a) and 50% for  $T_2^*$  (Figure 4b), as evident in the generated signal

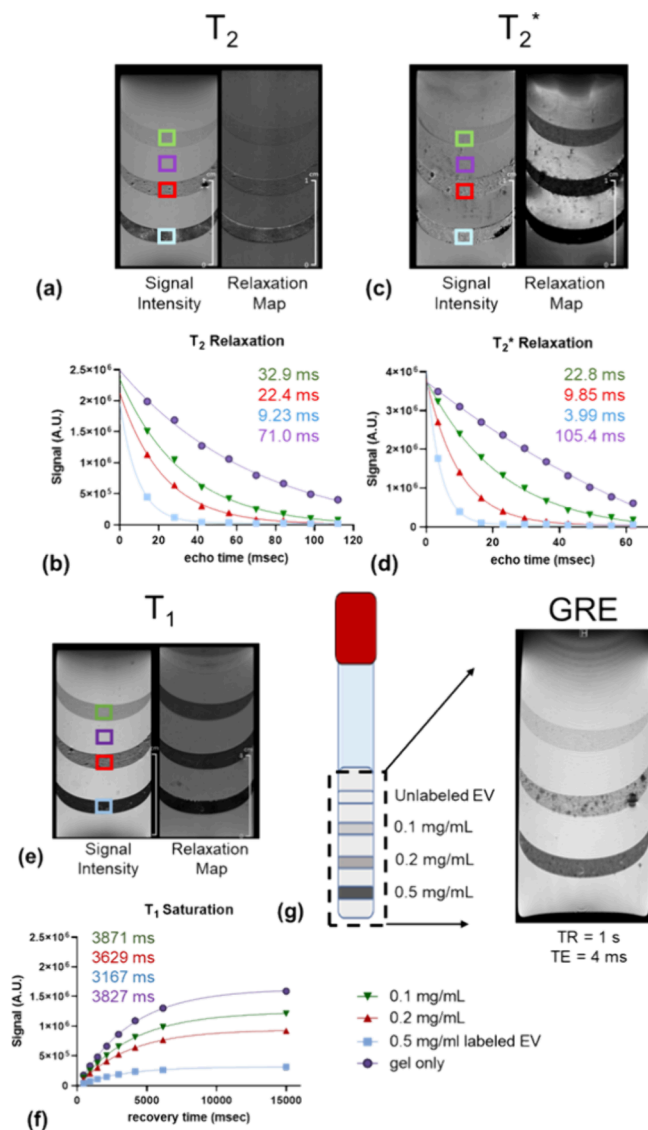


**Figure 4.** MRI of hMSC-EVs labeled and purified via Method 2 suspended in 1% agarose gel. (a,c,e) Signal intensity and relaxation maps for  $T_2$ ,  $T_2^*$ , and  $T_1$ , respectively. (b,d,f) Data fitted to exponential decay or saturation curves. (g) Schematic of EV samples in a 10 mm NMR tube (left) with blank 1% agarose in between layers and GRE image (right) of the NMR tube depicting contrast for bottom all three sample layers and no contrast for unlabeled EVs.

Table 2. Percent Contrast-to-Noise Ratio (Normalized to Gel)

method	USPIO incorporation	$T_2$ -weighted	$T_2^*$ -weighted	$T_1$ -weighted
		TE = 14 ms TR = 5 s	TE = 3.5 ms TR = 5 s	TE = 14 ms TR = 443 ms
1 (ExtraPEG)	0.5 mg/mL labeled EV	79.9%	50.0%	84.3%
	0.2 mg/mL labeled EV	44.4%	22.8%	43.1%
	0.1 mg/mL labeled EV	24.9%	7.67%	27.0%
2 (ultracentrifugation)	Condition A	46.8%	23.3%	51.5%
	Condition B	37.2%	27.8%	37.3%

intensity images, with exposure to 0.5 mg/mL USPIO. Supernatants of all samples displayed free USPIO and comparable signal loss indicating that all supernatants were saturated with labeling. Changes in CNR values for each EV sample compared to the gel are shown in Table 2.

### 3.3. In Vivo Visualization of USPIO-Labeled EVs.

hMSC-EVs using both labeling methods were suspended in PBS and administered to Sprague–Dawley rats immediately following 1 h MCAO-induced ischemia in the anatomical left hemisphere and subsequently imaged 1–4 h postinjection. This timing allowed the first passage imaging of the labeled EVs in the brain. The two methods were compared with EV-free USPIO injected under the same conditions.

Contrast levels stemming from USPIO (free and EV-incorporated) in live ischemic rats are demonstrated in Figure 5. EV-free USPIO resulted in some contrast in the striatal region at 1.3 h postinjection (Figure 5a). Histogram data fit to a normal distribution curve and mean signal intensity in both hemispheres following injection and approximately 24 h later confirmed a 17.8% decrease in the ipsilateral (ischemic) hemisphere (Figure 5b). This change stabilized both in mean intensity and a tighter distribution spread by 24 h. With Method 1 of EV labeling, in vivo imaging displayed large contrast areas near the left lateral and fourth ventricles at 3.3 h after injection, indicating a similar aggregation effect to that seen in phantoms, which was still prevalent ~24 h later (Figure 5c, white arrows indicate aggregated EV contrast). When analysis was restricted to the striatum, a 23.4% decrease in the mean signal intensity was evident in the ischemic hemisphere (Figure 5d). Although the mean intensity in the ischemic hemisphere moved toward the baseline 24 h later, a large shift was still evident. Alternatively, Method 2 provided visualization of the labeled EVs in the ischemic region 2 h postinjection (Figure 5e, white circles highlight diffused but strong contrast in the striatum) with minimal aggregation and a 22.6% decrease in mean signal intensity, which was cleared by 24 h (Figure 5f).

Studies have demonstrated that increased EV aggregation occurs when high centrifugation speeds are used in processing.<sup>44</sup> By incorporating PEG after the sonication step, the labeled EVs were allowed to be pelleted down at lower speeds, while free USPIO remained in the solution. In addition to the aggregation observed in vivo, the total distribution spread as well as mean signal intensity strongly supported preference for Method 2 in initial contrast generated immediately following injection as well as total clearance ~24 h later.

**3.4. Labeled hMSC-EV Purification Method Affects Therapeutic Potential.** The therapeutic efficacy of labeled EVs by both methods was evaluated with additional imaging sessions 1, 3, and 7 days postsurgery. Here, a hyper-intense signal in the  $^1\text{H}$   $T_2$ -weighted images acquired on day 1

confirmed the presence of an ischemic lesion in all rats (Figure 6a,b). The potential therapeutic efficacy of labeled EVs was established with  $^{23}\text{Na}$  MRI, specifically CSI, by measuring the ischemic lesion volume and  $^{23}\text{Na}$  signal corresponding to tissue sodium content (Figure 6c,d). Although the average lesion volume significantly reduced from day 3 to day 7 for Method 1 (Figure 6e), Method 2 maintained a higher level of fractional change over the entire 7-day time course (Figure 6f). Method 1 also resulted in a significant increase in lesion size compared to Method 2 according to fractional change analysis on days 1 to 3 (Figure 6f). Sodium signal within the lesion follows similar trends with Method 1 initially increasing, on average, 7.5% in sodium content from days 1 to 3 compared to an immediate 3.2% reduction for Method 2 (Figure 6h). Previous work has demonstrated that this reduction of lesion volume and sodium signal 72 h after ischemia induction and treatment administration indicates promising long-term recovery.<sup>27,43</sup>

## 4. DISCUSSION

Development of labeling strategies is essential to gain insight into the initial biodistribution and clearance of novel therapeutics, such as hMSC-EVs. Here, two methods of EV purification following labeling with MRI-visible USPIO via sonication were assessed. EV size distribution as well as protein and miRNA markers demonstrated that sonication did not greatly alter the EV bioprofile (i.e., size distribution, protein markers, and miRNA expression), which supports proper sonication procedures as a viable means of incorporating a labeling agent into hMSC-EVs while maintaining therapeutic potential.

However, the mechanical shear force from the sonicator probe may compromise the membrane integrity of the EVs while allowing USPIO into the EVs during membrane deformation. Alterations in protein cargo after EV sonication may exist, in particular, in the cytosol proteins. However, this membrane deformation process does not significantly affect the membrane-bound proteins. The protein cargo profile before and after EV sonication was analyzed by proteomics in our separate study (manuscript submitted), which shows the levels of protein cargo alteration by sonication. For the miRNA cargo profile, although the RT-PCR of specific miRNA did show the expression change after EV sonication, miRNA sequencing may need to be performed to examine the effect of sonication on global miRNA localization. Moreover, the lipidomics analysis can be performed in our future study to evaluate the effect of sonication on the lipid composition in the EVs. It is important to note that others have indicated alterations following EV sonication, particularly in size and morphology, indicating potential membrane integrity involvement that should be further evaluated in future studies.<sup>22,44</sup>

After USPIO integration, PEG enrichment and purification maintained a comparable EV bioprofile to the postsomication

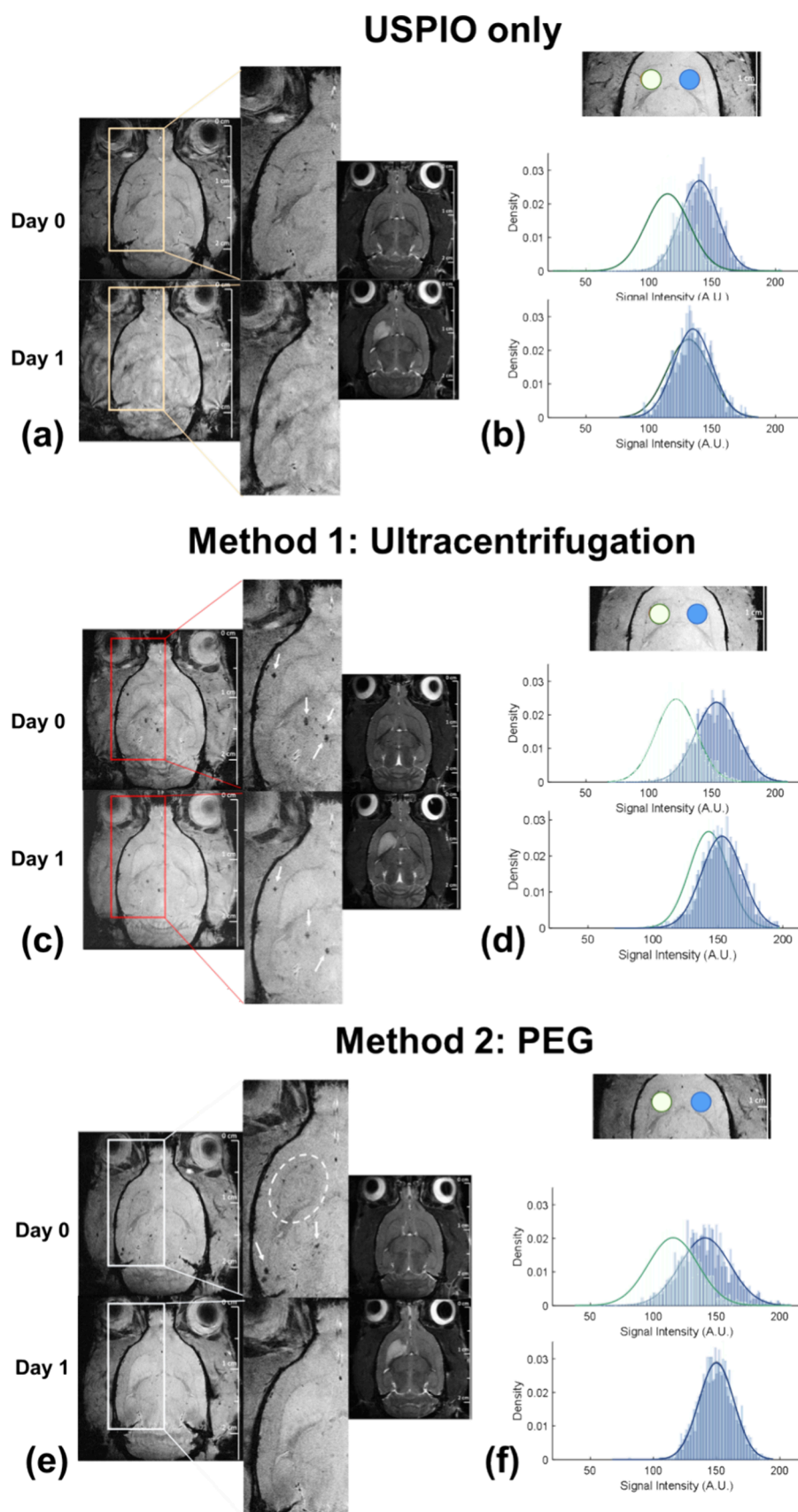


**Figure 5.** In vivo images of EV biodistribution and clearance on days 0 and 1. (a,c,e) GRE images of a representative animal on days 0 and 1 from each group. Boxes indicate the magnified striatal region in the ischemic hemisphere. White arrows indicate aggregated EV contrast and white circles highlight diffused but strong contrast in the striatum. (b,d,f) Signal intensities obtained from the striatum as indicated by colored circles in GRE images directly above histograms.

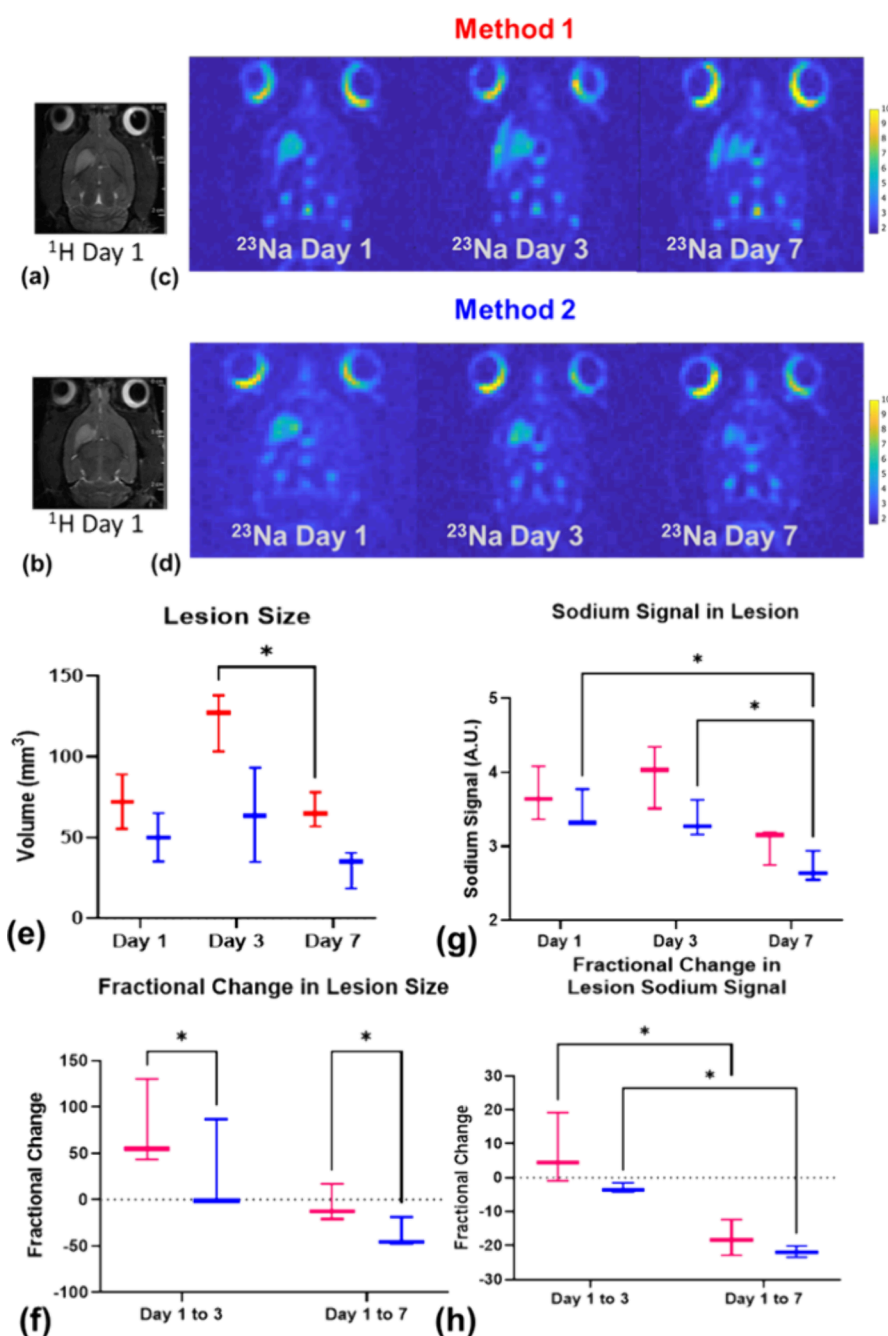


**Figure 6.** In vivo MRI of ischemic rats following administration of EVs labeled using Method 1 or 2. (a,b) Representative  $^1\text{H}$   $T_2$ -weighted images on day 1 with ischemic lesion in the left hemisphere. (c,d) Representative  $^{23}\text{Na}$  CSI generated on days 1, 3, and 7 with higher sodium signal indicated in yellow. (e) Lesion size as defined by  $^{23}\text{Na}$  ( $*p = 0.0279$ ) and (f) fractional changes in lesion size over time (days 1 to 3,  $*p = 0.0199$ ; days 1 to 7,  $*p = 0.0152$ ). (g) Average sodium signal intensity in the ischemic lesion (days 1 to 7,  $*p = 0.0143$ ; day 3 to 7,  $*p = 0.0304$ ) and (h) fractional changes over time (Method 1,  $*p = 0.0382$ ; Method 2,  $*p = 0.0202$ ). Statistical significance calculated using a mixed-effects model with Tukey's multiple comparison posthoc test ( $p < 0.05$ ). All values presented as mean  $\pm$  SD.

samples. PEG was previously shown to enrich and purify EVs as an alternative to other isolation methods, including differential centrifugation or costly commercial kits.<sup>30</sup> Rider et al. modified and improved the PEG enrichment method to preserve morphology, total protein, exosome-specific markers as well as RNA cargo in a high-recovery, low-specificity manner.<sup>30,45</sup> These functional molecules, particularly miRNA, promote neuroprotective properties including neurogenesis, neurite remodeling, and survival.<sup>46</sup> Previous studies have demonstrated therapeutic applications of selected miRNAs

applied to neurological disorders.<sup>47</sup> Specifically, miR-21 reduces neuronal apoptosis and improves neurological function in intracerebral hemorrhage.<sup>48</sup> When applied to focal cortical ischemia, enriched miR-124 delivery enhanced cortical neurogenesis.<sup>49</sup> Thus, the ExtraPEG enrichment that was performed throughout the isolation and labeling of hMSC-EVs to remove excess USPIO and the sonication of EVs to impart MRI detectability maintained the biological characteristics of hMSC-EVs that are key to preserving their therapeutic potential against ischemia.

Prior to *in vivo* applications, labeled hMSC-EVs prepared by using both ultracentrifugation and PEG methods were evaluated for MRI efficiency in brain-mimicking gels. USPIO are superparamagnetic iron oxide nanoparticles that shorten the transverse relaxation time of surrounding tissue, ultimately resulting in a measurable loss of signal and enhanced signal contrast.<sup>25,50,51</sup> Although both labeling methods achieved signal contrast, the PEG method greatly increased USPIO content, which was demonstrated in the  $T_2$ ,  $T_2^*$  values, and CNR calculations. The significant enhancement in contrast at comparable USPIO concentrations corresponds to a higher incorporated USPIO content for the ExtraPEG method. In fact, compared to Method 1, Method 2 using PEG exhibited a 3.6-fold enhancement in contrast using an equivalent USPIO concentration at 0.5 mg/mL and equivalent acquisition parameters (TE = 3.5 ms, TR = 5 s) when the dilution factor was considered. A dilution study indicated that as little as 0.1 mg/mL USPIO was necessary to visualize labeled EVs in gel phantoms using the PEG approach compared to the 0.5 mg/mL USPIO required using ultracentrifugation only. Furthermore, EV aggregation remained minimal utilizing the PEG approach with homogeneous layers demonstrated in the gel phantoms in contrast to the ultracentrifugation approach, which resulted in severe aggregate formation. It is noted that the free, unlabeled USPIO were present in the EV samples. Our study determined that the iron content of the EVs using USPIO labeling increased as determined by ICP. Potentially, density gradient ultracentrifugation can be used to better separate EV subpopulations and remove free USPIO from the labeled EV samples.<sup>47</sup>

Successful magnetic labeling allows MRI tracking of hMSC-EVs following systemic delivery during the first passage in the brain. Previous studies using alternative imaging modalities indicate that hMSC-EVs specifically target neurodegeneration.<sup>15</sup> Here, with direct application to a rat model of cerebral ischemia, MRI immediately following injection of USPIO-labeled EVs indicates localization within the affected striatal region and subsequent clearing of the MRI contrast within 24 h. However, the ultracentrifugation method exhibited EV aggregation *in vivo*, which could complicate therapeutic efficacy, including the potential to cause small blood clots and subsequent lacunar stroke lesions. Our study did not have an accurate measurement for the percentage of the injected EV dose that was found in the brain since this study did not investigate the biodistribution throughout the body. Specific experiments need to be designed to determine the *in vivo* EV dose in our future study.

Beyond successful labeling agent integration, *in vivo* preclinical evaluation of therapeutic efficacy provides the necessary foundation for further applications. Sodium MRI (<sup>23</sup>Na CSI) is a rigorous metric of tissue recovery in cerebral ischemia.<sup>27,43,52,53</sup> Ischemic stroke occurs when blood flow to a region of the brain is blocked, resulting in glucose and oxygen deprivation, which ultimately leads to cell swelling and sodium–potassium ATP pump dysregulation. As a result, the substantial increases in tissue sodium content in the affected region, primarily in the ischemic core and penumbra, is measurable with <sup>23</sup>Na MRI. Studies have demonstrated that <sup>23</sup>Na MRI is highly sensitive for assessing response to applied therapeutics in rat models of ischemic stroke.<sup>27,43</sup> By measurement of both ischemic lesion volume and sodium signal changes over time, a clear distinction between labeling methods was identified. The significantly improved tissue

recovery exhibited by the PEG labeling method suggests that this approach is more promising for future applications. This could be due to less disruption of the EV cargo during the sample preparation in the PEG method compared to the ultracentrifugation method. A more thorough omics-based EV cargo analysis may be required to verify this postulation. Moreover, PEG enrichment and purification of USPIO-labeled EVs demonstrate the feasibility of the large batch preparation of EVs as an alternative to direct cell therapy.

There are a few limitations that future studies should address. This study utilizes a single bolus intraarterial EV injection immediately following the transient ischemic occlusion to facilitate delivery and reduce animal discomfort during the subsequent recovery period. Although appropriate for evaluating the initial biodistribution and therapeutic benefits of labeled EVs, this approach only recapitulates the best-case scenario for the timing and application of treatments applied to clinical stroke. While the therapeutic evaluation performed here in the acute posts ischemic phase has shown promising outcomes in this preclinical setting, extended evaluation of tissue recovery is needed. Furthermore, additional evaluations of EV dose, the use of EVs from 3D cultures,<sup>47–49,54</sup> administration frequency, and delivery route will aid in establishing EVs as an optimal therapy.<sup>55</sup> In addition, the EV biodistribution throughout the body and ICP analysis of *ex vivo* organs, in particular the liver and spleen, are required for potential clinical applications. Moreover, further validation in a second animal model in addition to the MCAO model is required to demonstrate the therapeutic benefits of hMSC-EVs. Nevertheless, to our knowledge, this study is the first documented case of MR-sensitive, USPIO-labeled EVs applied to pathology within the central nervous system.

## 5. CONCLUSIONS

This study reports the development of a method to integrate USPIO nanoparticles as an MRI-visible contrast agent into hMSC-EVs. When applied to a preclinical cerebral ischemia model, the utilization of PEG to enrich and purify labeled EVs demonstrated superior contrast compared with EVs harvested by ultracentrifugation. Initial biodistribution and assessment of tissue recovery further support the therapeutic potential imparted by USPIO nanoparticle-labeled EVs derived from hMSCs. Although this study focuses on hMSC-EVs applied to cerebral ischemia due to stroke, the application of hMSC-EVs to other neurodegenerative diseases would be feasible as well.

## ■ ASSOCIATED CONTENT

### SI Supporting Information

The Supporting Information is available free of charge at <https://pubs.acs.org/doi/10.1021/acsnm.4c04888>.

Additional EV characterizations; EV size distribution; total protein content normalized to EV number; Ct values for a representative miRNA RT-PCR assay; donor information on bone marrow derived hMSCs; and size distribution of EV before and after sonication (PDF)

## ■ AUTHOR INFORMATION

### Corresponding Authors

Yan Li – Chemical & Biomedical Engineering, FAMU-FSU College of Engineering, Florida State University, Tallahassee, Florida 32310, United States; [orcid.org/0000-0002-5938-8519](https://orcid.org/0000-0002-5938-8519); Email: [yli@eng.famu.fsu.edu](mailto:yli@eng.famu.fsu.edu), [yli4@fsu.edu](mailto:yli4@fsu.edu)

**Samuel C. Grant** – National High Magnetic Field Laboratory and Chemical & Biomedical Engineering, FAMU-FSU College of Engineering, Florida State University, Tallahassee, Florida 32310, United States; [orcid.org/0000-0001-7738-168X](https://orcid.org/0000-0001-7738-168X); Phone: +1 850-645-7197; Email: [grant@magnet.fsu.edu](mailto:grant@magnet.fsu.edu); Fax: +1 530-706-4535

## Authors

**Shannon Helsper** – National High Magnetic Field Laboratory and Chemical & Biomedical Engineering, FAMU-FSU College of Engineering, Florida State University, Tallahassee, Florida 32310, United States; Present Address: Biomedical MRI at KU Leuven, 3000 Leuven, Belgium

**Xuegang Yuan** – National High Magnetic Field Laboratory and Chemical & Biomedical Engineering, FAMU-FSU College of Engineering, Florida State University, Tallahassee, Florida 32310, United States; Present Address: University of California, Los Angeles, California 90095, United States

**Richard Jeske** – Chemical & Biomedical Engineering, FAMU-FSU College of Engineering, Florida State University, Tallahassee, Florida 32310, United States; Present Address: Waters Corp, New Castle, Delaware 19720, United States

**Jamini Bhagu** – National High Magnetic Field Laboratory and Chemical & Biomedical Engineering, FAMU-FSU College of Engineering, Florida State University, Tallahassee, Florida 32310, United States

**Colin Esmonde** – Chemical & Biomedical Engineering, FAMU-FSU College of Engineering, Florida State University, Tallahassee, Florida 32310, United States

**Leanne Duke** – Department of Biomedical Sciences, College of Medicine, Florida State University, Tallahassee, Florida 32304, United States

**Li Sun** – Chemical & Biomedical Engineering, FAMU-FSU College of Engineering, Florida State University, Tallahassee, Florida 32310, United States; Department of Biomedical Sciences, College of Medicine, Florida State University, Tallahassee, Florida 32304, United States; [orcid.org/0000-0001-8228-7487](https://orcid.org/0000-0001-8228-7487)

Complete contact information is available at: <https://pubs.acs.org/10.1021/acsnm.4c04888>

## Notes

The authors declare no competing financial interest.

## ACKNOWLEDGMENTS

This study was funded by the US National Institutes of Health through the National Institute for Neurological Disorders and Stroke (RO1-NS102395 to S.C.G., RO1-NS125016 to Y.L., and F31-NS115409 to S.H.). Justice Ene helped illustration. The content is solely the responsibility of the authors and does not necessarily represent the official views of the National Institutes of Health. This study was supported partially by the US National Science Foundation (1743426 to Y.L.) and the Karen Toffler Charitable Trust (to X.Y.). A portion of this work was performed at the National High Magnetic Field Laboratory, which is supported by National Science Foundation Cooperative Agreement No. DMR-1644779 and the State of Florida.

## REFERENCES

(1) Raposo, G.; Stoorvogel, W. Extracellular vesicles: Exosomes, microvesicles, and friends. *J. Cell Biol.* **2013**, *200*, 373.

(2) Ludwig, A. K.; Giebel, B. Exosomes: Small vesicles participating in intercellular communication. *Int. J. Biochem. Cell Biol.* **2012**, *44*, 11–15.

(3) Boudna, M.; Campos, A. D.; Vychytilova-Faltejskova, P.; Machackova, T.; Slaby, O.; Souckova, K. Strategies for labelling of exogenous and endogenous extracellular vesicles and their application for in vitro and in vivo functional studies. *Cell Communication and Signaling* **2024**, *22*, 22.

(4) Dabrowska, S.; Del Fattore, A.; Karnas, E.; Frontczak-Baniewicz, M.; Kozłowska, H.; Muraca, M.; et al. Imaging of extracellular vesicles derived from human bone marrow mesenchymal stem cells using fluorescent and magnetic labels. *Int. J. Nanomed.* **2018**, *13*, 1653–1664.

(5) Buschmann, D.; Mussack, V.; Byrd, J. B. Separation, characterization, and standardization of extracellular vesicles for drug delivery applications. *Adv. Drug Delivery Rev.* **2021**, *174*, 348–368.

(6) Liu, W.; Li, L.; Rong, Y.; Qian, D.; Chen, J.; Zhou, Z.; et al. Hypoxic mesenchymal stem cell-derived exosomes promote bone fracture healing by the transfer of miR-126. *Acta Biomaterialia* **2020**, *103*, 196–212.

(7) Doeppner, T. R.; Herz, J.; Görgens, A.; Schlechter, J.; Ludwig, A.-K.; Radtke, S.; et al. Extracellular Vesicles Improve Post-Stroke Neuroregeneration and Prevent Postischemic Immunosuppression. *Stem Cells Translational Medicine* **2015**, *4*, 1131–1143.

(8) Hong, S. B.; Yang, H.; Manaenko, A.; Lu, J.; Mei, Q.; Hu, Q. Potential of Exosomes for the Treatment of Stroke. *Cell Transplant.* **2019**, *28*, 662–670.

(9) Saint-Pol, J.; Gosselet, F.; Duban-Deweer, S.; Pottiez, G.; Karamanos, Y. Targeting and Crossing the Blood-Brain Barrier with Extracellular Vesicles. *Cells* **2020**, *9*, 851.

(10) Gimona, M.; Pachler, K.; Laner-Plamberger, S.; Schallmoser, K.; Rohde, E. Manufacturing of Human Extracellular Vesicle-Based Therapeutics for Clinical Use. *Int. J. Mol. Sci.* **2017**, *18*, 1190.

(11) Otero-Ortega, L.; Laso-García, F.; Gómez-de Frutos, M. C.; Fuentes, B.; Diekhorst, L.; Díez-Tejedor, E.; et al. Role of Exosomes as a Treatment and Potential Biomarker for Stroke. *Translational Stroke Research* **2019**, *10*, 241–249.

(12) Otero-Ortega, L.; Carmen Gómez de Frutos, M.; Laso-García, F.; Rodríguez-Frutos, B.; Medina-Gutiérrez, E.; Antonio López, J.; et al. Exosomes promote restoration after an experimental animal model of intracerebral hemorrhage. *J. Cereb. Blood Flow Metab.* **2018**, *38*, 767–779.

(13) Zhang, Z. G.; Buller, B.; Chopp, M. Exosomes — beyond stem cells for restorative therapy in stroke and neurological injury. *Nature Reviews Neurology* **2019**, *15*, 193–203.

(14) Betzer, O.; Perets, N.; Angel, A.; Motiei, M.; Sadan, T.; Yadid, G.; et al. In Vivo Neuroimaging of Exosomes Using Gold Nanoparticles. *ACS Nano* **2017**, *11*, 10883–10893.

(15) Perets, N.; Betzer, O.; Shapira, R.; Brenstein, S.; Angel, A.; Sadan, T.; et al. Golden Exosomes Selectively Target Brain Pathologies in Neurodegenerative and Neurodevelopmental Disorders. *Nano Lett.* **2019**, *19*, 3422–3431.

(16) Lai, C. P.; Mardini, O.; Ericsson, M.; Prabhakar, S.; Maguire, C. A.; Chen, J. W.; et al. Dynamic Biodistribution of Extracellular Vesicles in Vivo Using a Multimodal Imaging Reporter. *ACS Nano* **2014**, *8*, 483–494.

(17) Busato, A.; Bonafede, R.; Bontempi, P.; Scambi, I.; Schiaffino, L.; Benati, D.; et al. Labeling and Magnetic Resonance Imaging of Exosomes Isolated from Adipose Stem Cells. *Curr. Protoc. Cell Biol.* **2017**, *75*, 3.44.1–3.44.15.

(18) Han, Z.; Liu, S.; Pei, Y.; Ding, Z.; Li, Y.; Wang, X.; et al. Highly efficient magnetic labelling allows MRI tracking of the homing of stem cell-derived extracellular vesicles following systemic delivery. *J. Extracell Vesicles* **2021**, *10*, No. e12054.

(19) Liu, T.; Zhu, Y.; Zhao, R.; Wei, X.; Xin, X. Visualization of exosomes from mesenchymal stem cells in vivo by magnetic resonance imaging. *Magn Reson Imaging* **2020**, *68*, 75–82.

(20) Sancho-Albero, M.; Ayaz, N.; Sebastian, V.; Chirizzi, C.; Encinas-Gimenez, M.; Neri, G.; et al. Superfluorinated Extracellular

Vesicles for In Vivo Imaging by 19F-MRI. *ACS Appl. Mater. Interfaces* **2023**, *15*, 8974–8985.

(21) Kutchy, N. A.; Ma, R.; Liu, Y.; Buch, S.; Hu, G. Extracellular Vesicle-Mediated Delivery of Ultrasmall Superparamagnetic Iron Oxide Nanoparticles to Mice Brain. *Front Pharmacol* **2022**, *13*, 13.

(22) Fu, S.; Wang, Y.; Xia, X.; Zheng, J. C. Exosome engineering: Current progress in cargo loading and targeted delivery. *NanoImpact* **2020**, *20*, No. 100261.

(23) Haney, M. J.; Klyachko, N. L.; Zhao, Y.; Gupta, R.; Plotnikova, E. G.; He, Z.; et al. Exosomes as drug delivery vehicles for Parkinson's disease therapy. *J. Controlled Release* **2015**, *207*, 18–30.

(24) Shapiro, E. M.; Sharer, K.; Skrtic, S.; Koretsky, A. P. In vivo detection of single cells by MRI. *Magn Reson Med.* **2006**, *55*, 242–249.

(25) Rosenberg, J. T.; Sellgren, K. L.; Sachi-Kocher, A.; Calixto Bejarano, F.; Baird, M. A.; Davidson, M. W.; et al. Magnetic resonance contrast and biological effects of intracellular superparamagnetic iron oxides on human mesenchymal stem cells with long-term culture and hypoxic exposure. *Cytotherapy* **2013**, *15*, 307–322.

(26) Helsper, S.; Yuan, X.; Bagdasarian, F. A.; Athey, J.; Li, Y.; Borlongan, C. V.; et al. Multinuclear MRI Reveals Early Efficacy of Stem Cell Therapy in Stroke. *Transl. Stroke Res.* **2023**, *14*, 545–561.

(27) Helsper, S.; Bagdasarian, A. F.; Yuan, X.; Xu, K.; Lee, J.-Y.; Rosenberg, J. T.; et al. Extended Ischemic Recovery After Implantation of Human Mesenchymal Stem Cell Aggregates Indicated by Sodium MRI at 21.1 T. *Transl Stroke Res.* **2022**, *13*, 543–555.

(28) Marzano, M.; Bou-Dargham, M. J.; Cone, A. S.; York, S.; Helsper, S.; Grant, S. C.; et al. Biogenesis of Extracellular Vesicles Produced from Human-Stem-Cell-Derived Cortical Spheroids Exposed to Iron Oxides. *ACS Biomater. Sci. Eng.* **2021**, *7*, 1111–1122.

(29) Busato, A.; Bonafede, R.; Bontempi, P.; Scambi, I.; Schiaffino, L.; Benati, D.; et al. Magnetic resonance imaging of ultrasmall superparamagnetic iron oxide-labeled exosomes from stem cells: a new method to obtain labeled exosomes. *Int. J. Nanomed.* **2016**, *11*, 2481–2490.

(30) Rider, M. A.; Hurwitz, S. N.; Meckes, D. G. ExtraPEG: A Polyethylene Glycol-Based Method for Enrichment of Extracellular Vesicles. *Sci. Rep.* **2016**, *6*, 23978.

(31) Hurwitz, S. N.; Meckes, D. G. An Adaptable Polyethylene Glycol-Based Workflow for Proteomic Analysis of Extracellular Vesicles. *Methods Mol. Biol.* **2017**, *1660*, 303–317.

(32) Wetterling, F.; Gallagher, L.; Mullin, J.; Holmes, W. M.; McCabe, C.; Macrae, I. M.; et al. Sodium-23 magnetic resonance imaging has potential for improving penumbra detection but not for estimating stroke onset time. *Journal of Cerebral Blood Flow and Metabolism* **2015**, *35*, 103–110.

(33) Liu, Y.; Tsai, A.-C.; Yuan, X.; Li, Y.; Ma, T. Hypoxia Regulation of Stem Cell. *Biology and Engineering of Stem Cell Niches, Elsevier* **2017**, 273–291.

(34) Yuan, X.; Logan, T. M.; Ma, T. Metabolism in human mesenchymal stromal cells: A missing link between HMSC biomanufacturing and therapy? *Front. Immunol.* **2019**, *10*, 977.

(35) Rosenberg, J. T.; Sachi-Koche, R. A.; Davidson, M. W.; Grant, S. C. Intracellular SPIO labeling of microglia: High field considerations and limitations for MR microscopy. *Contrast Media Mol. Imaging* **2012**, *7*, 121–129.

(36) Longa, E. Z.; Weinstein, P. R.; Carlson, S.; Cummins, R. Reversible middle cerebral artery occlusion without craniectomy in rats. *Stroke* **1989**, *20*, 84–91.

(37) Fu, R.; Brey, W. W.; Shetty, K.; Gorōkov, P.; Saha, S.; Long, J. R.; et al. Ultra-wide bore 900 MHz high-resolution NMR at the National High Magnetic Field Laboratory. *J. Magn. Reson.* **2005**, *177*, 1–8.

(38) Kowal, J.; Arras, G.; Colombo, M.; Jouve, M.; Morath, J. P.; Primdal-Bengtson, B.; et al. Proteomic comparison defines novel markers to characterize heterogeneous populations of extracellular vesicle subtypes. *Proc. Natl. Acad. Sci. U.S.A.* **2016**, *113*, E968–E977.

(39) Deng, H.; Sun, C.; Sun, Y.; Li, H.; Yang, L.; Wu, D.; et al. Lipid, Protein, and MicroRNA Composition Within Mesenchymal Stem Cell-Derived Exosomes. *Cellular Reprogramming* **2018**, *20*, 178–186.

(40) Ji, Q.; Ji, Y.; Peng, J.; Zhou, X.; Chen, X.; Zhao, H.; et al. Increased brain-specific MiR-9 and MiR-124 in the serum exosomes of acute ischemic stroke patients. *PLoS One* **2016**, *11*, No. e0163645.

(41) Yu, P.; Chen, W. Advances in the diagnosis of exosomal miRNAs in ischemic stroke. *Neuropsychiatric Disease and Treatment* **2019**, *15*, 2339.

(42) Linares, R.; Tan, S.; Gounou, C.; Arraud, N.; Brisson, A. R. High-speed centrifugation induces aggregation of extracellular vesicles. *Journal of Extracellular Vesicles* **2015**, *4*, 4.

(43) Yuan, X.; Rosenberg, J. T.; Liu, Y.; Grant, S. C.; Ma, T. Aggregation of human mesenchymal stem cells enhances survival and efficacy in stroke treatment. *Cytotherapy* **2019**, *21*, 1033–1048.

(44) Nizamudeen, Z. A.; Xerri, R.; Parmenter, C.; Suain, K.; Markus, R.; Chakrabarti, L.; et al. Low-Power Sonication Can Alter Extracellular Vesicle Size and Properties. *Cells* **2021**, *10*, 2413.

(45) Théry, C.; Witwer, K. W.; Aikawa, E.; Alcaraz, M. J.; Anderson, J. D.; Andriantsitohaina, R.; et al. Minimal information for studies of extracellular vesicles 2018 (MISEV2018): a position statement of the International Society for Extracellular Vesicles and update of the MISEV2014 guidelines. *Journal of Extracellular Vesicles* **2018**, *7*, 7.

(46) Nasirishargh, A.; Kumar, P.; Ramasubramanian, L.; Clark, K.; Hao, D.; Lazar, S. V.; et al. Exosomal microRNAs from mesenchymal stem/stromal cells: Biology and applications in neuroprotection. *World Journal of Stem Cells* **2021**, *13*, 776.

(47) Yuan, X.; Sun, L.; Jeske, R.; Nkosi, D.; York, S.; Liu, Y.; Grant, S. C.; Meckes, D. G.; Li, Y. Engineering Extracellular Vesicles by Three-dimensional Dynamic Culture of Human Mesenchymal Stem Cells. *J. Extracell. Vesicles* **2022**, *11* (6), No. e12235.

(48) Zhang, H.; Wang, Y.; Lv, Q.; Gao, J.; Hu, L.; He, Z. MicroRNA-21 overexpression promotes the neuroprotective efficacy of mesenchymal stem cells for treatment of intracerebral hemorrhage. *Frontiers in Neurology* **2018**, *9*, 1–13.

(49) Yang, J.; Zhang, X.; Chen, X.; Wang, L.; Yang, G. Exosome Mediated Delivery of miR-124 Promotes Neurogenesis after Ischemia. *Molecular Therapy Nucleic Acids* **2017**, *7*, 278–287.

(50) Padmanabhan, P.; Kumar, A.; Kumar, S.; Chaudhary, R. K.; Gulyás, B. Nanoparticles in practice for molecular-imaging applications: An overview. *Acta Biomaterialia* **2016**, *41*, 1–16.

(51) Zhi, D.; Yang, T.; Yang, J.; Fu, S.; Zhang, S. Targeting strategies for superparamagnetic iron oxide nanoparticles in cancer therapy. *Acta Biomaterialia* **2020**, *102*, 13–34.

(52) Madelin, G.; Lee, J.-S.; Regatte, R. R.; Jerschow, A. Sodium MRI: methods and applications. *Prog. Nucl. Magn. Reson. Spectrosc.* **2014**, *79*, 14–47.

(53) Boada, F. E.; Qian, Y.; Nemoto, E.; Jovin, T.; Jungreis, C.; Jones, S. C.; et al. Sodium MRI and the Assessment of Irreversible Tissue Damage During Hyper-Acute Stroke. *Translational Stroke Research* **2012**, *3*, 236–245.

(54) Liu, C.; Sun, L.; Worden, H.; Ene, J.; Zeng, O. Z.; Bhagu, J.; Grant, S. C.; Bao, X.; Jung, S.; Li, Y. Profiling biomanufactured extracellular vesicles of human forebrain spheroids in a Vertical Wheel bioreactor. *J. Extracell. Biol.* **2024**, *3*, No. e70002.

(55) Welsh, J. A.; Goberdhan, D. C. I.; O'Driscoll, L.; Buzas, E. I.; Blenkiron, C.; Bussolati, B.; Cai, H.; Di Vizio, D.; et al. Minimal information for studies of extracellular vesicles (MISEV2023): From basic to advanced approaches. *J. Extracell. Vesicles* **2024**, *13* (2), No. e12404.